MACHINE BUILDING AND MACHINE SCIENCE

УДК 621.791.75:004.942 https://doi.org/10.23947/2687-1653-2020-20-3-259-268

Physicomathematical modeling of the formation features of fillet welds of bridge metal structures under submerged-arc welding

A. A. Mosin[1], V. A. Erofeev[2], M. A. Sholokhov[3]
[1] "Kurganstalmost" CJSC (Kurgan, Russian Federation)
[2] Tula State University (Tula, Russian Federation)
[3] Ural Federal University named after the First President of Russia B.N. Yeltsin (Ekaterinburg, Russian Federation)

Introduction. The weld formation under the submerged-arc welding of bridge metal structures is investigated. The work objective is to study possibilities to increase the welding performance during the arc welding of fillet seams.
Materials and Methods. Methods of computer analysis are used to optimize the technology. With their help, a physicomathematical model of fillet weld formation under the submerged-arc welding has been developed. It is based on a system of equations for thermal conductivity and equilibrium of the weld pool surface. In this system, the formation of an arc cavern is determined through the flux boiling isotherm under the action of the arc column radiation; heat transfer by the flux vapor inside the arc cavern and the influence of the spatial position on the formation of the weld pool are taken into account.
Results. New mathematical relationships that describe physical phenomena under the submerged-arc welding of fillet welds are proposed. The key feature of the proposed model is in the fundamental difference between the submerged-arc welding and the gas-shielded arc welding, i.e., during submerged-arc welding, the arc burns in a gas-vapor cavern that appears due to the melting and evaporation of flux. Numerical simulation of the temperature distribution during production of the fillet welds in 1F and 2F positions is carried out. The process constraints under the single-run welding of the fillet welds are specified. It was determined that the single-run submerged-arc welding of fillet welds in 1F position exhibits high-quality formation of welds for almost the entire range of metal sheet thicknesses. During production of fillet welds in 2F position, high-quality formation is provided only for sheet thicknesses up to 8 mm. At heavy thicknesses, the formation of the seam is disrupted due to the melt flow from the vertical wall. In this case, the leg length decreases; a typical undercut is formed; so the weld will be asymmetric and less strong.
Discussion and Conclusions. Comparison of the numerical analysis results with actual data on welding modes under the production of bridge metal structures shows that the existing fillet welding technologies have already reached their maximum efficiency rate. Further productivity gain is possible by forming oversized legs only with multiarc or multielectrode welding methods.

Keywords: fillet weld, submerged-arc welding, physicomathematical model, numerical simulation, arc cavern.

For citation: A.A. Mosin, V.A. Erofeev, M.A. Sholokhov. Physicomathematical modeling of the formation features of fillet welds of bridge metal structures under submerged arc welding. Advanced Engineering Research, 2020, vol. 20, no. 3, p. 259−268. https://doi.org/10.23947/2687-1653-2020-20-3-259-268

Introduction. Traditional methods of bridge construction provide for the enlarged assembly of bulk welded metal structures at the construction site [1]. Therefore, at the facility itself, welding work is carried out to a minimum. They are performed mainly at the factories of bridge metal structures [2], and most of them are associated with the welding of elongated seams. Of these, corner welds account for 40% to 70%. Fillet welding with small thickness is carried out without grooving. For thicknesses up to 50 mm, asymmetric and symmetrical grooves with an included angle of 45-60 ° are used. Fillet welds with a flat surface in cross section and smooth transitions to the base metal along the fusion zones without sagging and undercuts, gas cavities and slag inclusions are optimal. In addition, weld joints should have high ductility and impact toughness at low temperatures. Defects in the formation of seams are unacceptable. Sound reproduction of the maximum possible leg, when welding fillet seams, is the main capacity for increasing productivity [3].

To minimize defects and increase the productivity of welding processes for bridge metal structures, it is advisable to weld fillet seams with the largest possible leg size in one pass. Therefore, an urgent task is to increase the leg welded in one pass [4]. This can be achieved through the following:

— optimization of the parameters of welding processes,
— using new sources of heating,
— reduction of auxiliary time,
— increasing the fusibility of the electrode wire.

In our opinion, first of all, one should consider the possibility of a sound shop reproduction of the maximum possible leg using the traditional submerged-arc consumable-electrode welding technology.

This work objective is to study the possibilities of increasing the productivity of the arc welding process of fillet welds with account of the characteristic properties of their formation.

Materials and Methods. As noted in [5], in addition to the well-known parameters of the welding mode (arc current, welding speed), the performance of the submerged-arc welding process is influenced by the arc voltage and the diameter of the electrode wire. The spatial position during welding and the positioning of the electrode in the groove also affect significantly the formation of fillet welds [6]. It is a highly time-consuming task to consider the influence of the entire set of the listed factors on the productivity of the welding process and the quality of fillet welds without using modern research methods.

For a significant reduction in the volume of experimental studies of fillet welding, physicomathematical modeling of stresses and features of shaping and penetration is used [7–9]. Let us consider the sequence of computer simulation of the features of the formation of fillet welds — from creating a model to its visualization. The principle difference between the submerged-arc welding method and gas shielded arc welding is that the arc burns in a vapor-gas cavity arising from the melting and evaporation of the flux. The second important feature is that physical phenomena determining the formation of the weld pool and seam occur in different environments [9]. This should be taken into account in the physicomathematical model of the seam formation under the submerged-arc welding.

Modeling space coordinates. When modeling, the space in which fillet welding is performed, and the geometric dimensions of high-quality welds are specified. In Fig. 1*a,* an area of space covering the welded edges and zones of arc burning, melting of the flux and metal is highlighted; and in Fig. 1*b,* geometric dimensions of fillet welds, which can be used to assess the quality of their formation in accordance with the recommendations, are shown [5].

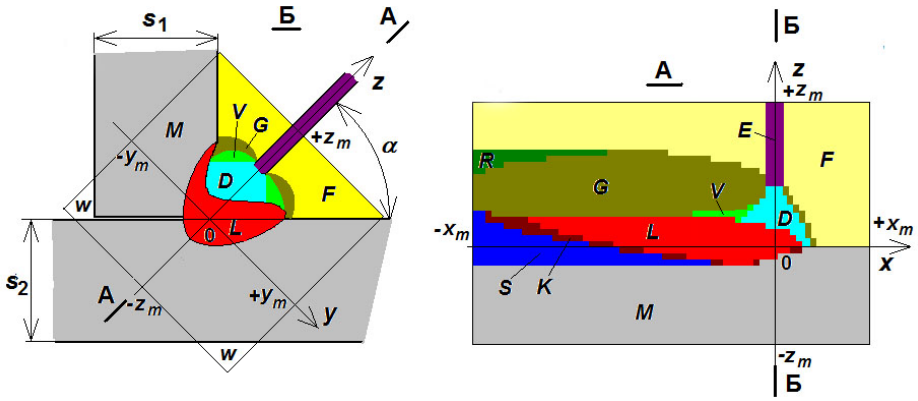

a)

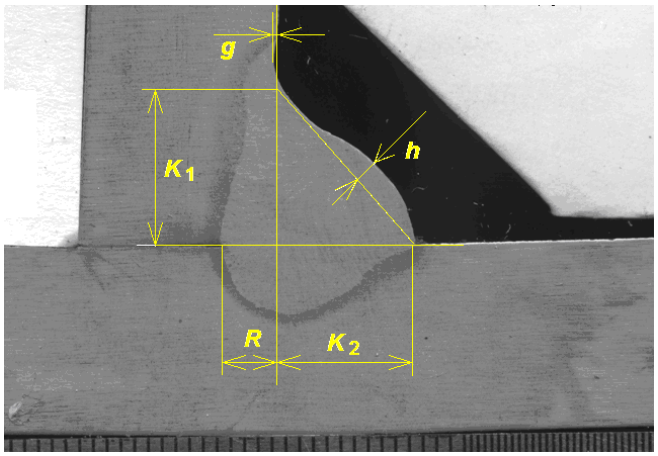

b)

Fig. 1. Structure of the simulation space for the welding process (*a*), and the geometric dimensions of fillet welds (*b*), which determine the quality of their formation

The simulation space includes the following zones: *M* — parent metal, *E* — electrode, *D* — welding arc, *F* — free flow flux, *V* — flux vapor, *G* — molten flux, *R* — solidified flux, *L* — liquid metal, *K* — solid-liquid metal, *S* — weld metal, *W* — air. Internal interzone surfaces are designated as intersections of sets of points belonging to the corresponding zones.

For example, the surface of the weld pool Z_L (x, y) is designated $L\cap(D\cup V\cup G)$. It separates the weld pool *L* from the welding arc *D*, the vaporous *V* and liquid *G* flux. The sizes of the *V, G, L, K* zones and the location of the interfaces between them are unknown. They need to be defined under the simulation. These indicators depend on the results of solving the system of equations describing physical phenomena of the submerged-arc welding. It is more convenient to solve such a problem in a fixed Cartesian coordinate system, in which the metal of the welded joint is stationary, and the electrode and arc move at the welding speed v_w in the direction of the *x* coordinate. Accordingly, the coordinates of the electrode axis x_f and y_f are determined:

$$H_{i,j,k}(t)=H_{i+1,j,k}(t-\tau), \tag{1}$$

where *t* is time since excitation.

When welding, the surfaces of fillets and interface zone are oriented mainly in the plane connecting the fillet weld legs. It is convenient to describe such surfaces as a deviation from this plane. Therefore, the *z* coordinate is directed along the bisector α of the angle between the sheets (or the groove angle).

Heat transfer is a common process for all designated areas. The simulation considers the thermodynamic state of media with different thermophysical properties, in which several internal local distributed heat sources operate. The rate of change and distribution of enthalpy should be described from the equation [10]:

$$\frac{\partial H}{\partial t}=\frac{\partial}{\partial x}\left(\lambda\frac{\partial T}{\partial x}\right)+\frac{\partial}{\partial y}\left(\lambda\frac{\partial T}{\partial y}\right)+\frac{\partial}{\partial z}\left(\lambda\frac{\partial T}{\partial z}\right)+q\,(x, y, z, t). \tag{2}$$

Here, $H = H\,(x, y, z, t)$ is volumetric enthalpy, J/cm^3; $\lambda = \lambda(T)$ is heat conductivity factor dependent on temperature and material of the medium, W/(cm·°C); q is volumetric heat source. The temperature $T\,(x, y, z, t)$ is related to the enthalpy $H\,(x, y, z, t)$ by the nonlinear function $T(H)$, which takes into account the dependence of the heat capacity on the temperature and heat of phase and aggregate transformations. At the initial moment of time, the weld pool is absent, the flux is in a free flow state, the temperature at all points in space is the same and equal to the ambient temperature. Taking this into account, the heat exchange between the simulation zone and the external space can be described by the boundary conditions:

$$\frac{\partial^2 T}{\partial x^2}=0,\ x=\pm x_m, \tag{3}$$

$$\frac{\partial^2 T}{\partial y^2}=0,\ y=\pm y_m, \tag{4}$$

$$\frac{\partial^2 T}{\partial z^2}=0,\ z=\pm z_m. \tag{5}$$

Heat sources. The main heat sources are the electric arc q_{arc} acting in zone *D*, and the heat released under the electrode stickout [11, 12]. Heat release in the liquid flux is close to non-existent, since it has no direct contact with the electrode whose temperature is lower than the melting point of the flux, and the electrical resistance of the powder flux is very high. Taking these circumstances into account, the heating rate of the metal in the electrode stickout (in zone *E*) can be described by the relation:

$$\frac{\mathrm{d}T_f}{\mathrm{d}z}=\frac{\rho_e j^2}{c\rho_f}\frac{z_m-z}{v_f} \tag{6}$$

where T_f is temperature of the stickout; $\rho_e = \rho_e(T_f)$ is electrical resistivity; $j=\frac{4I}{\pi d_f^2}$ is current density *I* in the electrode of diameter d_f; $c\rho_f$ is volumetric heat capacity of the electrode material; v_f is the wire feed speed.

Heat release in the anodic region of the arc on the surface $E\cap D$ is described as the heat flux:

$$\frac{dq}{dz}=jU_a, \tag{7}$$

where U_a is voltage drop in the anode region of the arc.

Heat release in the plasma arc flame is considered as the distribution of the arc column radiation over the surface of the arc cavern $L\cap(D\cup V)$:

$$\frac{\partial^2 T}{\partial y^2}=0, y=\pm y_{n'}. \tag{8}$$

The heat flux created by heat release in the cathode region of the arc on the surface $L\cap D$ is:

$$\frac{dq}{dn}=\frac{IU_k}{\pi R^2}\exp\left(\frac{-r_0^2}{R^2}\right), \tag{9}$$

where U_k is cathode arc voltage, *R* is effective radius of the arc, r_0 is the distance between the surface point $L\cap D$ and the point of intersection of the arc axis and this surface.

Heat transfer by drops of electrode metal is considered by the heat flux through the surface $L\cap D$ [13]:

$$\frac{dq}{dn}=\frac{IT_k}{\pi R^2}\exp\left(\frac{-r_0^2}{R^2}\right), \tag{10}$$

where T_k is droplet temperature taken equal to the half-sum of the melting and boiling temperatures of the electrode material.

Heat transfer by flux vapor is described as heat flux through the surface of the weld pool $L \cap V$ and flux $G \cap V$: $\frac{\partial^2 T}{\partial z^2} = 0, z = \pm z_m$. The heat transfer coefficient is determined from the balance of the capacities of evaporation and condensation of steam:

$$\int_{S_Z} \frac{dq}{dn} dS_Z \overrightarrow{p\,\mathrm{vap} = \mathrm{var}} 0, \tag{11}$$

where S_z is the area of specified surfaces $L \cap V \cup G \cap V$.

Equilibrium equation of the weld pool surface. The location of the weld pool surface $Z(x, y)$, delimiting the zones $L \cap (D \cup V \cup G)$, is determined by solving the pressure equilibrium equation on it:

— capillary p_σ,

— gravitational p_g,

— stream of electrode metal drops p_f,

— hydrodynamic pressure of the weld pool metal flow p_v,

— electrodynamic pressure of the arc p_a,

— internal pressure of liquid metal p_m.

$$\frac{dT_f}{dz} = \frac{\rho_e j^2}{c\rho_f} \frac{z_m - z}{v_f}. \tag{12}$$

Capillary pressure is determined by the curvature of the surface $Z(x, y)$, and for small deflections, it is calculated:

$$p_\sigma = -\sigma \left(\frac{\partial^2 Z}{\partial x^2} + \frac{\partial^2 Z}{\partial y^2} \right), \tag{13}$$

where σ is the surface tension constant.

Gravitational pressure is determined by the weight of a column of substance above a point on the surface of the weld pool:

$$p_g = \mathrm{g}(\rho(Z - z_{\max}) + \rho_h Z_h), \tag{14}$$

where g is acceleration of gravity; ρ, ρ_h are densities of metal and slag; z_{max} is maximum height of the weld pool surface; Z_h is thickness of the liquid slag layer.

Electrodynamic pressure of the welding arc is determined by the arc current:

$$p_a = \frac{k_a I^2}{\pi R_p^2} \exp\left[-\frac{(x_0 + v_w t)^2 + y^2}{R_p^2} \right], \tag{15}$$

where k_a is the electrodynamic coefficient, R_p is force radius of the arc.

Flow pressure of electrode metal droplets is determined by the flow rate and mass:

$$p_f = \rho \frac{v_f^2}{2} \exp\left[\frac{-(x_0 + v_w t)^2 + y^2}{R_f^2} \right]. \tag{16}$$

Hydrodynamic pressure of the weld pool metal flow is determined by the rate of change in the weld pool section area S_L:

$$p_v = -\rho v_x^2 \frac{dS_L}{dx}. \tag{17}$$

This component increases the pressure in front of the arc and decreases it behind the arc.

Internal pressure in the melt p_m is determined from the equality of the deposited metal area to the amount of consumed electrode metal:

$$S_{S \cup M}(-x_m) - S_M(+x_m) \overrightarrow{p_m = var} \pi r_f \frac{v_f}{v_w}, \tag{18}$$

where $S_{S \cup M}(-x_m)$ is the cross-sectional area of the metal at the end of the simulation area at $x = -x_m$; $S_M(x)$ is the initial groove cross-sectional area at $x = x_m$.

Current and location of the welding arc. The welding arc current I is set by the feed rate v_f and the diameter d_f of the electrode:

$$I = v_f \frac{\pi d_f^2}{4} \left(c\rho_f (T_k - T_f) + H_{LS} \right), \tag{19}$$

where T_k is temperature of the electrode metal droplets; H_{LS} is the volumetric specific heat of fusion.

The length l of the welding arc is set by the voltage U_0 of the power source and depends on the electrical resistance of the current-carrying elements R_0 and the stickout of the electrode R_f:

$$l = 1/E\,(U_0 - U_a - U_k - I\,(R_0 + R_f)). \tag{20}$$

The arc length l is determined by the potential gradient E in the arc column whose value depends on the properties of the flux vapor. With curved surface $L \cap D$ of the cathode spot, the concept of arc length needs to be clarified. If we consider the arc column as a set of parallel conductors, then the current density will be the greater, the smaller the distance from the electrode tip to the point of the metal surface. The average length l of the set of such conductors can be determined by solving the equation:

$$\sqrt{\frac{1}{S}\int_0^S \frac{1}{r^2}\,dS} = \frac{1}{l}. \quad (21)$$

Here, r is the distance from the electrode tip to the considered point of the weld pool surface; S is the cross-sectional area of the column determined by the effective radius R of the arc. The radius depends on the current I of the arc [13]:

$$R = \sqrt{\frac{I}{\pi j} + R_f^2},$$

where j is the current density in the arc in flux vapors.

Electrical resistance of the stickout depends on its length L_f and temperature T_f distributed along the length:

$$R_f = \frac{4}{\pi d_f^2}\int_0^{L_f} \rho_e\big(T_f(z)\,dz\big). \quad (22)$$

Algorithm for the numerical solution to the system of equations of the physicomathematical model. Initially, the geometric structure of the weld pool formation zone is unknown. This requires continuous adjustment of the location of the interzone surfaces depending on the results of solving the equations of thermal conductivity and equilibrium of the weld pool. The location of the surfaces delimiting the solid, liquid and gaseous state of the flux and metal is specified by the position of the corresponding isotherms as a result of solving the heat conduction equation. To correct the location of the weld pool surface, the equation of pressure equilibrium on the given surface $Z(x, y)$ is solved. In this case, it is required to change the sizes of the zones *L, V, G, D*. It is assumed that the temperatures of the metal and slag in the displacement zone are equal to the surface temperature at the time of the solution, and their enthalpies change in accordance with this temperature. During the transformation, errors arise, which are defined as the rate of change in enthalpy when changing the volumes v_L, v_G of zones L and G:

$$\Lambda_L = \frac{d}{dt}\Big(\int_{v_L} H dv_L\Big) \text{ и } \Lambda_G = \frac{d}{dt}\Big(\int_{v_G} H dv_G\Big). \quad (23)$$

These errors are compensated for a change in the enthalpy of the L and G zones depending on the temperature distribution in them:

$$\frac{d}{dt}H\big((x, y, z) \in L\big) = \Lambda_L \frac{T(x, y, z) - T_L}{\frac{1}{v_L}\int_{v_L}(T(x, y, z) - T_L)\,dv_L}, \quad (24)$$

where T_L is the liquidus temperature.

As the thermodynamic state approaches the steady state, the transformation error is $\Lambda_L \to 0$. The condition for the simulation termination is stabilization of the solidus isotherm length:

$$\frac{d}{dt}(\max x \in S) \to 0. \quad (25)$$

The model system of equations is solved by the temperature distribution $T(x, y, z, t)$ and the geometric structure of the simulation zone. This provides reproducing the initial stage of the process from the arc starting moment until the established dimensions of the weld pool are reached. To solve the equations of thermal conductivity and equilibrium of the weld pool surface, the finite-difference method on conjugate meshes was used. On the interphase surfaces, the thermal conductivity coefficient was determined as the average harmonic value of the thermal conductivity of adjacent phases.

An algorithm for the numerical simulation of the welding process is schematically presented below.

Initial data: groove geometry after the previous pass, thermophysical properties of steel and flux, welding parameters
Determination of the initial geometry of the numerical solution domain Calculation of melting parameters of the electrode wire and energy characteristics of the welding arc
Cycle of unsteady numerical simulation of the thermodynamic state of the weld pool formation region
Determination of the distribution of heat fluxes over the surfaces of metal and slag Solving the heat equation
Solution to the variational problem on the location of welding arc in the groove
Solution to the equilibrium equation of the weld pool surface under the action of capillary, gravitational, electrodynamic, hydrodynamic and internal pressures
Calculation of the weld pool internal pressure by the condition of the balance of seam masses and electrode feed
to equal masses of surfacing and electrode feed
Correction of the location of the interphase boundaries of "vapor - slag – free flow flux - solid slag", "solid - liquid metal" according to the solutions to the equation of thermal conductivity and equilibrium of the surface of the weld pool
until the length of the solidus temperature isotherm stabilizes
Formation of a protocol of simulation results on temperature distribution, geometry of the weld pool formation area, energy characteristics of the welding process

Fig. 2. Algorithm for numerical simulation of the weld formation under the submerged-arc welding

Research Results. For a virtual study, we took information on the thermophysical properties of steels from [13]. In addition, we used the data of the Transstroiinvest corporate group on the specific steel grades and technological materials used, the modes of submerged-arc fillet welding of bridge metal structures[1].

Virtual reproduction of the welding process in 1F position. To test the developed model, we performed computer simulation of the T-joint welding of 15KHSND T1steel sheets 12 mm thick. The welding mode was chosen according to the recommendations [14]: Sv08GA wire with a diameter of 5 mm, arc voltage — 34 V, welding speed — 18 m/h (5 mm/s), electrode stickout — 25 mm. The electrode feed rate, calculated in the model, is 10 mm/s. This corresponds to the data of [14], which recommends these values in the range of 55–61 m/h.

Fig. 3 shows the results of welding simulation when the sheets are tilted 45° (1F position).

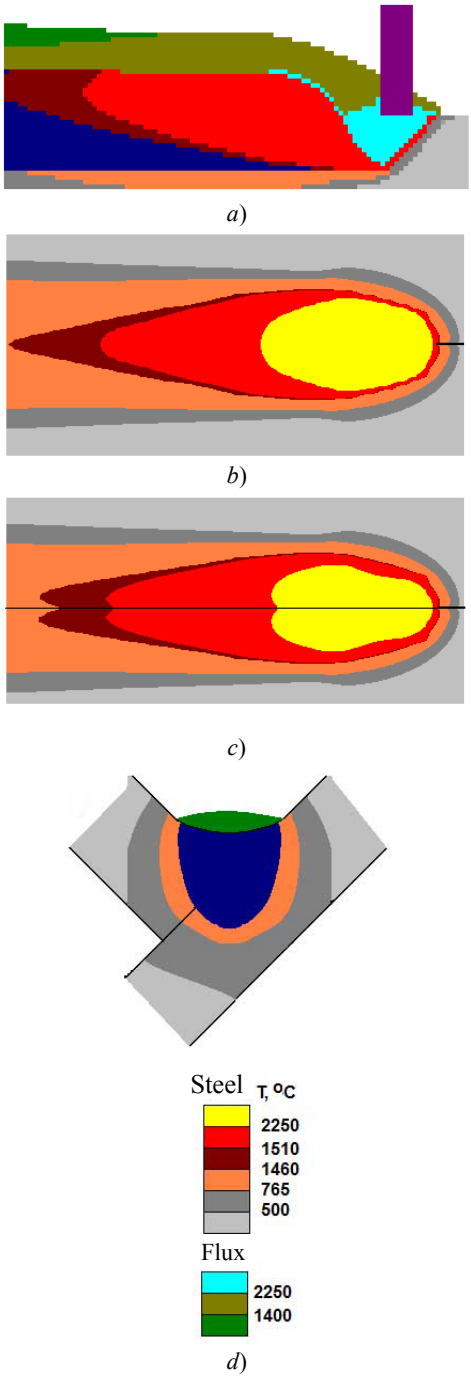

Fig. 3. Temperature distribution under submerged-arc fillet welding simulation when the sheets are tilted at 45° (1F position):
(a) longitudinal section of the weld pool in the plane of joint symmetry;
(b) submerged metal surface); (c) surface of the sheets to be welded;
(d) calculated cross-sectional profile of the seam

[1] STO-GK “Transstroi” -012-2007. Steel structures of bridges. Factory production. Moscow: Transstroy; 2007. 174 p. (In Russ.)

As a result, the following values were obtained: arc length — 6.8 mm; effective drop of anode voltage — 5.9 V, that of cathode voltage — 8.5 V; potential gradient in the arc column — 4.4 V/mm; arc column diameter — 18 mm. The total power of the process is 23 kW, of which 12.9 kW is radiation. The arc emits 4.3 kW at the electrode; 5.8 kW — at the joint surface. Heat dissipation power at the electrode stickout is 0.2 kW; the temperature of its heating by the arc current is 152°C. The area of the arc cavern plan is 135 mm^2; cavern volume is 519 mm^3. The crater depth under the arc is 16 mm. The length of the weld pool on the surface along the liquidus is 38 mm, along the solidus — 52 mm. The welding pool weight is 150 g. Seam width is 15 mm; the leg is 10.7 mm; the joint penetration depth is 6 mm; the cross-sectional area is158 mm^2. The weld is formed with a meniscus up to 1.3 mm.

Virtual simulation of the corner welding process. When welding large structures, it is impossible to use rotators. In this case, corner welding is performed. The simulation result of the formation of a weld at this position and under the same conditions is shown in Fig. 4.

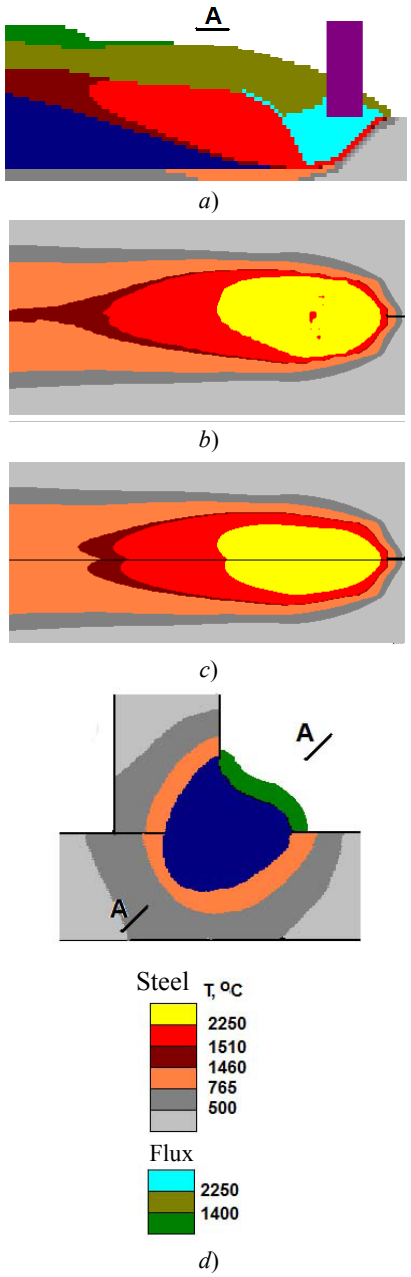

Fig. 4. The computer simulation result of the fillet weld formation under corner welding with welding of a vertical wall to a horizontal base: (*a*) longitudinal section of the weld pool in the symmetry plane of the joint; (*b*) submerged metal surface; (c) surface of weld sheets; (*d*) design weld cross-sectional profile

A noticeable melt flow from the butt wall to the flange under the corner welding is due to large mass of the weld pool. The deviation of the seam surface from the plane connecting the walls is ± 1.5 mm. The melt flows from the vertical wall to the horizontal base, so the weld is asymmetric, and the melt in the upper part of the weld is reduced by 2 mm.

The largest possible leg size. It needs to be specified at what maximum leg size ("1F position" and "corner"

welding) a high-quality seam is formed. For this purpose, we simulated fillet welding of 8 mm thick sheets with a 2 mm diameter wire at an arc current of 350 A. The welding speed and arc voltage were varied. The results are shown in Fig. 5.

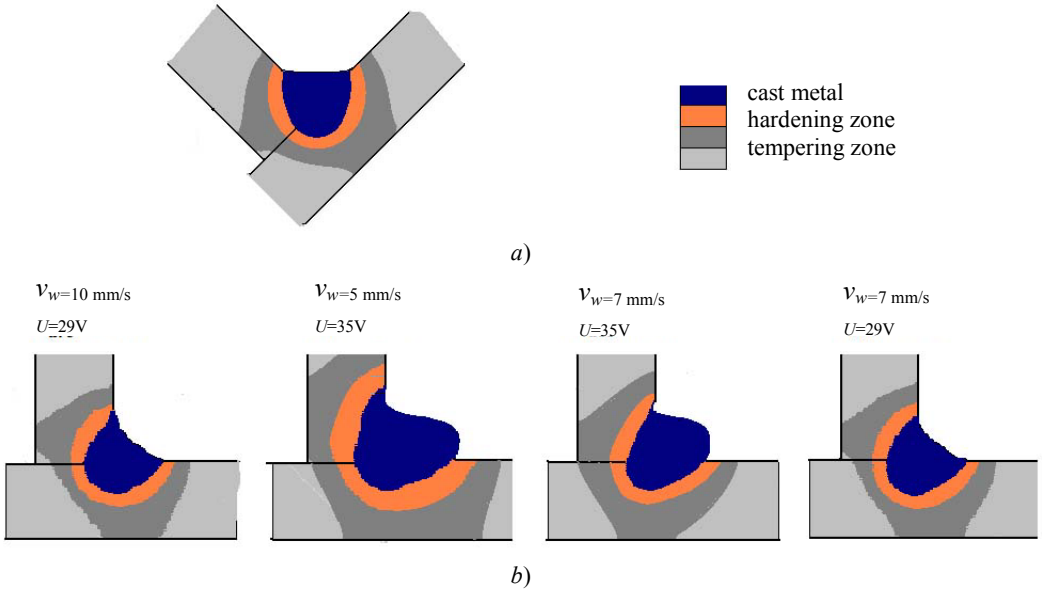

Fig. 5. Result of computer simulation of seam formation:
(*a*) 1F position, (*b*) corner

If the recommended 1F position welding speed is observed (Fig. 5*a*), a seam with equal legs of 6 mm is formed. This is less than required, but without collaring and meniscus. Under the corner welding in the same mode (Fig. 5*b*), a seam with meniscus is formed. To increase the leg, simulations were performed at a lower welding speed and a higher arc voltage value. At a speed of 5 mm/s and a voltage of 35 V, the cross-sectional area of the cast zone and its dimensions increase dramatically, but a seam is formed with an undercut and collar. Increasing the welding speed up to 7 mm/s reduces collaring. If the tension is reduced, an acceptable seam is formed with the legs of about 7 mm.

These results show that the recommended submerged arc welding modes are the most productive for obtaining legs of a given size. To obtain larger legs under single-arc welding, additional passes are required. However, in this case, the overall welding performance is significantly reduced.

Discussion and Conclusions. Labor intensity of manufacturing elements of bridge structures is largely determined by labor intensity of welding. A rational way to increase productivity is to use automatic submerged-arc welding. To optimize the technology using computer analysis methods, a physicomathematical model of forming fillet welds under submerged-arc welding has been developed. The model is based on a system of equations for heat conductivity and equilibrium of the weld pool surface. In this system, the formation of an arc cavern is determined by the boiling isotherm of the flux under the action of radiation from the arc column. Heat transfer by flux vapors inside the arc cavity and the influence of the spatial position on the formation of the weld pool are taken into account. The equations of the model of submerged-arc welding of fillet joint with metal thickness typical for bridge structures are solved numerically. The solution shows that when performing 1F position welding, the joint is formed in one pass. According to the simulation data, when welding a fillet weld “into a corner”, unsatisfactory formation is possible due to the flow of liquid metal from the vertical wall. In this case, additional backing passes are required to obtain a high-quality seam.

The studies have shown that the traditional technology of single-arc submerged-arc fillet welding with the formation of oversized legs has already reached its maximum productivity. To further increase it, it is required to use more complex advanced techniques. Such unconventional technologies include:

— multi-arc and multi-electrode welding methods [14, 15],

— introduction of non-conducting filler wire (cold wire feed welding) [16], granular metal additive (grit) or metal powder into the weld pool [17].

References

1. Kurlyand VG, Kurlyand VV. Stroitel'stvo mostov: ucheb. posob. dlya vuzov [Bridge Engineering]. Moscow: MADI; 2012. 176 p. (In Russ.)

2. Poloskov SS, Zheltenkov AV. Organizatsionno-upravlencheskii mekhanizm upravleniya innovatsionnym potentsialom vysokotekhnologichnykh naukoemkikh predpriyatii [Organizational and economic mechanism of management of innovative potential for high-tech knowledge intensive enterprises]. Economy and Entrepreneurship. 2019;2(103):1051–1057. (In Russ.)

3. Votinova EB, Shalimov MP, Fiveiskii AM. Osnovy tekhnologicheskoi podgotovki proizvodstva [Basics of technological preparation of production]. Ekaterinburg: URFU; 2017. 168 p. (In Russ.)

4. Mosin AA. Vozmozhnosti povysheniya proizvoditel'nosti svarki protyazhennykh uglovykh shvov mostovykh metallokonstruktsii [Ways to solve problems of increasing the efficiency of welding long corner seams of three-dimensional metal structures]. Welding and Diagnostics. 2020;1:50–54. (In Russ.)

5. Artemov AO, Karatysh VV, Yazovskikh VM, et al. Issledovanie vliyaniya rezhimov svarki pod sloem flyusa na formu i proplavlenie uglovykh shvov [Investigation of the effect of submerged-arc welding modes on the shape and penetration of fillet welds]. Bulletin of Perm University. Machine Building, Materials Sciences. 2010;12(5):130–142. (In Russ.)

6. Tomas KI, Il'yashchenko DP. Tekhnologiya svarochnogo proizvodstva [Welding technology]. Tomsk: Izd-vo TPU; 2011. 247 p. (In Russ.)

7. Shen J, Chen Z. Welding simulation of fillet-welded joint using shell elements with section integration. Journal of Materials Processing Technology. 2014;214(11):2529–2536.

8. Cho D-W, Song W-H, Cho M-H, et al. Analysis of submerged arc welding process by three-dimensional computational fluid dynamics simulations. Journal of Materials Processing Technology. 2013;213(12):2278–2291.

9. Sudnik VA, Erofeev VA, Maslennikov AV, et al. Matematicheskaya model' protsessa svarki pod flyusom i yavlenii v dugovoi kaverne [Mathematical model of the submerged-arc welding process and phenomena in the arc cavern]. Svarochnoe Proizvodstvo. 2012;7:3–12. (In Russ.)

10. Sudnik VA, Erofeev VA, Maslennikov AV. Matematicheskaya model' formirovaniya svarochnoi vanny pri dugovoi svarke pod flyusom i analiz protsessa perenosa metalla [Mathematical model of the weld pool formation in the saw-process and analysis of the electrode metal transfer]. Izvestiya TulGU. 2015;6(2):21–31. (In Russ.)

11. Ghosh A, Chattopadhyay H. Mathematical modeling of moving heat source shape for submerged arc welding process. The International Journal of Advanced Manufacturing Technology. 2013;6:2691–2701.

12. Leskov GI. Ehlektricheskaya svarochnaya duga [Electric welding arc]. Moscow: Mashinostroenie; 1970. 355 p. (In Russ.)

13. Taits NYu. Tekhnologiya nagreva stali [Steel heating technology]. Moscow: Metallurgizdat; 1962. 568 p. (In Russ.)

14. Mel'nikov AYu, Fiveiskii AM, Sholokhov MA, et al. Inzhenernaya metodika rascheta parametrov rezhima dvukhdugovoi svarki uglovykh shvov [Engineering method for calculating the parameters of the mode of double-arc welding of fillet welds]. Welding and Diagnostics. 2016;3:46–48. (In Russ.)

15. Kiran DV, Cho D-W, Song W-H, et al. Arc interaction and molten pool behavior in the three wire submerged arc welding process. International Journal of Heat and Mass Transfer. 2015;87:327–340.

16. Ribeiro RA, Dos Santos EBF, Assunção PDC, et al. Predicting weld bead geometry in the novel CW-GMAW process. Welding Journal. 2015;94(9):301–311.

17. Ivochkin II, Malyshev BD. Svarka pod flyusom s dopolnitel'noi prisadkoi [Submerged arc welding with additional additive]. Moscow: Stroiizdat; 1981. 176 p. (In Russ.)

Submitted 30.04.2020
Scheduled in the issue 06.07.2020

About the Authors:

Mosin, Aleksei A., Deputy Director for Production, "Kurganstalmost" CJSC (3, Zagorodnaya St., Kurgan, 640023, RF), ORCID: https://orcid.org/0000-0002-5809-5423, Mosinaa@kurganstalmost.ru.

Erofeev, Vladimir A., professor of the Welding, Casting and Construction Materials Technology Department, Tula State University (92, Lenin Pr., Tula, 300012, RF), Cand.Sci. (Eng.), ORCID: https://orcid.org/0000-0003-3756-2640, Va_erofeev@mail.ru.

Sholokhov, Mikhail A., Head of the Automation and Robotization of Welding Production Department, Yeltsin Ural Federal University (UrFU) (19, Mira St., Ekaterinburg, 620002, RF), Cand.Sci. (Eng.), ORCID: https://orcid.org/0000-0002-7666-5645, M.a.sholokhov@urfu.ru.

Claimed contributorship

A. A. Mosin: research objectives and task setting; determination of the modeling area and boundary conditions; analysis of the research results; text preparation; formulation of conclusions. V. A. Erofeev: building of the physicomathematical model; analysis of the research results. M. A. Sholokhov: academic advising; the text revision; correction of the conclusions.

All authors have read and approved the final manuscript.